International Journal of Biological Macromolecules 226 (2023) 37–50

Contents lists available at ScienceDirect

International Journal of Biological Macromolecules

journal homepage: www.elsevier.com/locate/ijbiomac

The pursuit of new alternative ways to eradicate *Helicobacter pylori* continues: Detailed characterization of interactions in the adenylosuccinate synthetase active site

Ante Bubić [a], Marta Narczyk [b], Ana Petek [c], Marta Ilona Wojtyś [b,d], Weronika Maksymiuk [b], Beata Wielgus-Kutrowska [b], Maria Winiewska-Szajewska [b], Tea Pavkov-Keller [e,f,g], Branimir Bertoša [c], Zoran Štefanić [a], Marija Luić [a], Agnieszka Bzowska [b,*], Ivana Leščić Ašler [a,*]

[a] Department of Physical Chemistry, Ruđer Bošković Institute, Bijenička cesta 54, HR-10000 Zagreb, Croatia
[b] Division of Biophysics, Institute of Experimental Physics, Faculty of Physics, University of Warsaw, Pasteura 5, 02-093 Warsaw, Poland
[c] Department of Chemistry, Faculty of Science, University of Zagreb, Horvatovac 102A, HR-10000 Zagreb, Croatia
[d] Department of Bacterial Genetics, Institute of Microbiology, Faculty of Biology, University of Warsaw, Miecznikowa 1, 02-096 Warsaw, Poland
[e] Institute of Molecular Biosciences, University of Graz, Humboldtstraße 50/III, 8010 Graz, Austria
[f] BioTechMed-Graz, Mozartgasse 12/II, Graz 8010, Austria
[g] BioHealth Field of Excellence, University of Graz, Humboldtstrasse 50, 8010 Graz, Austria

ARTICLE INFO

Keywords:
Helicobacter pylori
Adenylosuccinate synthetase
Substrate (inhibitor) binding
Enzyme kinetics
X-ray structure
Molecular dynamics

ABSTRACT

Purine nucleotide synthesis is realised only through the salvage pathway in pathogenic bacterium *Helicobacter pylori*. Therefore, the enzymes of this pathway, among them also the adenylosuccinate synthetase (AdSS), present potential new drug targets. This paper describes characterization of His_6-tagged AdSS from *H. pylori*. Thorough analysis of 3D-structures of fully ligated AdSS (in a complex with guanosine diphosphate, 6-phosphoryl-inosine monophosphate, hadacidin and Mg^{2+}) and AdSS in a complex with inosine monophosphate (IMP) only, enabled identification of active site interactions crucial for ligand binding and enzyme activity. Combination of experimental and molecular dynamics (MD) simulations data, particularly emphasized the importance of hydrogen bond Arg135-IMP for enzyme dimerization and active site formation. The synergistic effect of substrates (IMP and guanosine triphosphate) binding was suggested by MD simulations. Several flexible elements of the structure (loops) are stabilized by the presence of IMP alone, however loops comprising residues 287–293 and 40–44 occupy different positions in two solved *H. pylori* AdSS structures. MD simulations discovered the hydrogen bond network that stabilizes the closed conformation of the residues 40–50 loop, only in the presence of IMP. Presented findings provide a solid basis for the design of new AdSS inhibitors as potential drugs against *H. pylori*.

1. Introduction

Bacterium *Helicobacter pylori* has been evolving alongside humans for millennia, originating in east Africa as well as our ancestors [1]. Identified only in 1984 [2], this gram-negative microaerophilic bacterium is now recognized as the class I human carcinogen [3] and its involvement in the development of several serious diseases (chronic active gastritis, peptic ulceration, gastric adenocarcinoma, and gastric mucosa-associated lymphoid tissue lymphoma) is evidenced [4]. Nowadays, it is estimated that about half of the world's population is infected with *H. pylori*, mostly asymptomatic [5].

During its long cohabitation with humans, *H. pylori* has developed the tools for surviving the harsh conditions of human stomach – helical shape, flagella, burying inside gastric mucous layer, excreting urease, to mention just a few [6]. Also, its metabolism was optimised for living in a relatively stable environment of a human host, by reducing the redundancy in metabolic pathways that is often found in environmental microbes [7]. One of these reduced metabolic pathways is the synthesis of purine nucleotides. While most organisms have both de novo purine nucleotide biosynthesis and purine salvage pathways, allowing the generation of DNA and RNA in the absence and presence of external purine sources, respectively, *H. pylori* possesses genes for enzymes of

* Corresponding authors.
E-mail addresses: Agnieszka.Bzowska@fuw.edu.pl (A. Bzowska), ivana.lescic.asler@irb.hr (I. Leščić Ašler).

https://doi.org/10.1016/j.ijbiomac.2022.12.001
Received 15 June 2022; Received in revised form 11 November 2022; Accepted 1 December 2022
Available online 5 December 2022

purine salvage pathway only [8].

In our group, the investigation is focused on two enzymes of the purine salvage pathway: purine nucleoside phosphorylase (PNP) and adenylosuccinate synthetase (AdSS) [9–13]. PNP (EC 2.4.2.1) catalyses the reversible phosphorolytic cleavage of the glycosidic bond of purine ribo- and deoxyribonucleosides:

(deoxy)purine nucleoside + orthophosphate ↔ purine base + (2′-deoxy)ribose-1-phosphate.

Bacterial PNPs mainly belong to the "high molecular mass" PNPs (M_r in the range of 110–150 kDa) that are homohexamers accepting as substrates both 6-oxo- and 6-aminopurine nucleosides [14]. Thus, they differ from "low molecular mass" PNPs ($M_r \sim 90$ kDa) which are trimers specific for 6-oxopurine nucleosides and are found mainly in mammals [14]. Ubiquitous enzyme AdSS (EC 6.3.4.4) has a role in both pathways of purine production, catalysing the first step in the biosynthesis of AMP from IMP, namely conjugation of IMP and aspartate to form adenylosuccinate (AMPS):

IMP + Asp + GTP (Mg^{2+}) ↔ adenylosuccinate + GDP + P_i.

In the next step, adenylosuccinate lyase cleaves adenylosuccinate to form AMP. While vertebrates have two isoforms of AdSS, acidic and basic, bacteria produce only one, similar in properties to the acidic isoform of vertebrates' enzyme [15]. AdSSs are generally functional dimers with $M_r \sim 90$–100 kDa. Due to its critical point in the metabolism of purines, substrate binding sites of AdSS are quite specific for its designated substrates [16].

The research of Liechti and Goldberg [7] on the growth of *H. pylori* mutants with deletions of purine salvage pathway enzymes on media supplemented with various purine nucleosides and bases has indicated that both PNP and AdSS are essential for purine nucleotide synthesis in this bacterium. Also, as mutants with deletions of these enzymes are unable to grow on a complementary set of purine bases/nucleosides [7], simultaneous treatment with inhibitors of both enzymes could completely abolish bacterium's growth. Indeed, synergistic therapy (use of a combination of two or more substances, which when used together directly or indirectly increase the effectiveness of the treatment) is standard therapy for eradicating *H. pylori*, and new possibilities are investigated in this line of research [17]. New lines of attack on *H. pylori* are of vital importance, knowing that standard therapy at the moment usually consists of a proton pump inhibitor and two antibiotics (mostly clarithromycin and amoxicillin or metronidazole), and its efficacy is estimated to be even <60–70 %, mainly due to the increasing level of antibiotic resistance [18].

A total of 50 3D-structures of AdSS enzymes from 15 different organisms are available in Protein Data Bank (May 2022). The core of the protein is essentially invariant in all of the structures, comprising a β-sheet of 9 strands, surrounded by domains forming the active site. Structures of fully ligated enzymes (i.e. with all three substrates/substrate analogues bound) are virtually identical [19–21]. However, for the basic isoform of mouse AdSS and *E. coli* AdSS several structures are solved of protein complexed with various combinations of substrates/inhibitors (i.e. not fully ligated), which enabled identification of conformational differences in the active site that contribute to different substrate recognition of these enzymes [21]. So, pinpointing these subtle differences in the active site between human and pathogen's AdSS enzymes could significantly enhance the process of rational drug design, and a detailed analysis of the pathogen's active site is the first step in this direction.

Biochemical characterization of the native *H. pylori* AdSS was published previously [11]. In this article, the study on interactions of the His-tagged variant of this enzyme with its substrates and inhibitors is presented, investigated through kinetic parameters, binding constants, 3D-structure and molecular dynamics simulations.

2. Materials and methods

2.1. Preparation of H. pylori AdSS-His

Plasmid bearing gene coding for *H. pylori* AdSS including His_6-tag on C-terminus was prepared by inversed polymerase chain reaction (PCR) from previously prepared *pET21b-HPpurA* plasmid [11]. Primers used: forward – 5′-TAGAAAAATCGTGTCTTCTC-3′, reverse – 5′-CTCGAG-CACCACCAC-3′. Phusion Flash High-Fidelity PCR Master Mix 2X (New England Biolabs) was used, according to manufacturer's instructions. The resulting plasmid, *pET21b-HPpurA-His* was subcloned by electroporation into *E. coli* cell strain BL21-CodonPlus(DE3)-RIL (Agilent Biotechnology, Santa Clara, CA) which was used for expression of the recombinant *H. pylori* AdSS-His. Enzyme expression was performed in the LB medium containing 100 mg/mL of ampicillin. The cells were grown at 37 °C and 220 rpm to $OD_{600nm} \sim 0.6$ and expression was induced with 0.5 mM IPTG (Isopropyl β-D-1-thiogalactopyranoside) and proceeded overnight at 18 °C and 220 rpm. Cells were harvested at 5000 ×*g*, at 4 °C.

Protein purification was performed at 4 °C. Cells were resuspended in 50 mM Na-phosphate buffer pH 8.0 containing 0.5 M NaCl and 10 mM imidazole (buffer A), to which also 0.1 mM phenylmethylsulfonyl fluoride (PMSF) was added. High-pressure homogenizer (Avestin Emulsiflex C3) was used to lyse the cells. Cell debris was separated from protein extract by centrifugation for 20 min at 15,000 ×*g*, at 4 °C. Three mL of Ni-NTA agarose (Protino, Macherey-Nagel) equilibrated in buffer A was added to the clear supernatant. After 30 min of incubation, agarose was poured into the purification column and washed with 20 mL of buffer A. After another washing step (20 mL of buffer B - 50 mM Na-phosphate buffer pH 8.0 containing 0.5 M NaCl and 20 mM imidazole), bound proteins were eluted with 9 mL of buffer C (50 mM Na-phosphate buffer pH 8.0 containing 0.5 M NaCl and 300 mM imidazole). For additional purification of AdSS and removal of any possible aggregates or protein fragments, size-exclusion chromatography (SEC) was performed. Sephacryl S-200 16/60 column (Cytiva Life Sciences) was equilibrated in 20 mM Hepes (2-[4-(2-hydroxyethyl)piperazin-1-yl] ethane-1-sulfonic acid) buffer pH 7.0 containing 150 mM NaCl and 1 mM β-mercaptoethanol, and operated at 0.6 mL/min on the ÄKTA protein purification system (Cytiva Life Sciences). Two millilitres of the concentrated sample were loaded onto the column, and fractions of 2 mL were collected. The final sample of purified AdSS (in SEC buffer) was concentrated to 25 mg/mL and stored in aliquots at −80 °C until use.

The purification was monitored by electrophoresis under denaturing conditions (as described in Section 2.2.) and a protein concentration assay following the method of Bradford [22] with bovine serum albumin as a standard. For purified protein samples, protein concentration was determined utilizing protein's molar extinction coefficient at 280 nm of 38,850 M^{-1} cm^{-1} (as calculated by the ProtParam tool at ExPasy.org).

SEC was also used to estimate the molecular mass/oligomeric state of *H. pylori* AdSS-His (under the conditions described). The column was calibrated with several proteins from the Gel Filtration Calibration Kit (Cytiva Life Sciences) – chymotrypsinogen A (25 kDa), yeast alcohol dehydrogenase (37.5 kDa), bovine serum albumin (67 kDa), catalase (232 kDa) and ferritin (440 kDa), together with Blue Dextran. The elution volume of the marker proteins was determined by absorption detection at 280 nm.

2.2. Electrophoresis under denaturing conditions

The purification of *H. pylori* AdSS-His was followed by electrophoresis under denaturing conditions (sodium dodecyl sulfate–polyacrylamide gel electrophoresis, SDS-PAGE). Two systems were used. Horizontal SDS-PAGE was performed on a PhastSystem apparatus (Cytiva Life Sciences). PhastGel 12.5 % plates and SDS buffer strips were used, both from the same producer, as well as the protein low molecular weight (LMW) markers (14.4–97.0 kDa). Vertical SDS-PAGE was

performed in a Mini-PROTEAN Tetra Cell (Bio-Rad). Gels (Laemmli, 12.5 %) for this system were cast in-house. LMW markers were also used in this system. Prior to loading, samples were mixed with treatment buffer (PhastSystem – 20 mM Tris–HCl pH 8.0, 2 mM ethylenediaminetetraacetic acid (EDTA), 5 % SDS, 10 % 2-mercaptoethanol; Mini-PROTEAN system – 0.125 M Tris–HCl pH 6.8, 4 % SDS, 20 % glycerol, 2 % 2-mercaptoethanol) in ratio 1:1 (*v*/v) and heated for 5 min at 95 °C. Gels were stained with Coomassie Brilliant Blue R-250.

2.3. Analytical ultracentrifugation

The oligomeric properties of *H. pylori* AdSS-His were studied by analytical centrifugation with absorbance detection at 225 nm, using the sedimentation velocity method. Optima XL-I ultracentrifuge (Beckman-Coulter Inc., Indianapolis, IN), An-50Ti and An-60Ti analytical rotors, and double-sector 1.2-cm cells with Epon-charcoal centrepieces with sapphire or quartz windows were used. Experiments were conducted at 142,000 ×*g*, at 20 °C, in 20 mM Hepes pH 6.8–7.0 buffer, with tris(2-carboxyethyl)phosphine (TCEP) 1 or 2 mM, and NaCl 0 or 150 mM. The partial specific volume of *H. pylori* AdSS from the amino acid composition, densities and viscosities of buffers were calculated using the Sednterp program [23]. The protein samples (390 μL) had a concentration of 19.4–70 μg/mL (i.e., 0.4–1.5 μM in terms of enzyme subunits).

Radial scans of the absorption profiles in the centerpiece cell were measured at 7-min intervals. Analysis of the ultracentrifugation data was done by the Sedfit program using the continuous c(s) distribution model [24]. The sedimentation coefficient fitting range was 0–15 S. Both the sedimentation coefficient, s and the standard sedimentation coefficient, $s^0_{20,w}$ were calculated, and based on them the molecular mass of the species present in the solution was determined, assuming that they have the same friction ratio (also obtained as a parameter in the Sedfit program).

2.4. Enzyme activity assay

Enzyme activity assay was performed as described before [11], in 1 mL reaction mixture in 20 mM Hepes buffer pH 7.7, at room temperature (~25 °C), with saturating substrate concentrations (guanosine triphosphate, GTP at 0.06 mM, inosine monophosphate, IMP at 0.15 mM and sodium aspartate, Asp at 5 mM) and 1 mM Mg^{2+}, utilizing molar extinction coefficient at 280 nm of 1.17×10^4 M^{-1} cm^{-1} (formation of adenylosuccinate) [25].

One unit (U) of AdSS enzymatic activity is defined as μmol of adenylosuccinate formed per min at 25 °C, in given conditions. Specific activity is expressed as units per mg of protein (U/mg).

When AdSS-His was tested for pH and temperature stability, the enzyme was incubated in 0.1 mg/mL concentration, either at different temperatures in 20 mM Hepes buffer pH 7.7 or in Britton–Robinson universal buffer of different pH [26] at 25 °C. After 1 h, 10 μL of incubation mixture was used for each activity measurement under standard conditions (20 mM Hepes buffer pH 7.7, at room temperature).

2.5. Determination of kinetic constants

Kinetic constants of *H. pylori* AdSS-His were determined in the same manner as for the native AdSS [11]. Briefly, enzyme activity was measured while the concentration of one substrate was varied, and concentrations of the other two substrates were kept constant (GTP at 0.06 mM, IMP at 0.15 mM and Asp at 5 mM). The experimentally obtained data were analyzed by fits of the Michaelis–Menten equation using GraphPad Prism version 8.0 (GraphPad Software, Inc., San Diego, CA).

To determine the inhibition constant value, K_i, of guanosine diphosphate (GDP), concentrations of Asp and IMP were maintained at saturating levels (5 and 0.15 mM, respectively), while initial concentrations of GTP and GDP were varied from 3 to 120 μM and from 1 to 6 μM, respectively. The data were analyzed by fits of the competitive inhibition model using GraphPad Prism version 8.0.

Table 1
Data collection and refinement statistics of *H. pylori* AdSS structures.

	AdSS-full	AdSS-IMP
PDB code	6ZXQ	7PVO
Wavelength (Å)	1.00	1.54
Resolution range (Å)	48.46–1.4 (1.45–1.4)[a]	23.79–2.00 (2.05–2.00)
Space group	*C* 2	*I* 2
Unit cell (Å, °)	120.706, 68.362, 68.828 90.00, 121.113, 90.00	69.105, 61.326, 119.636 90.00, 98.42, 90.00
Total reflections	615,933 (61,088)	455,787 (23,078)
Unique reflections	93,429 (9246)	33,613 (2477)
Multiplicity	6.6 (6.6)	13.6 (9.3)
Completeness (%)	99.10 (98.08)	99.9 (100)
Mean $I/\sigma I$	8.11 (1.11)	38.7 (9.7)
Wilson B-factor	17.8	12.8
R_{merge}	0.13 (1.49)	0.05 (0.21)
R_{meas}	0.14 (1.61)	0.05 (0.23)
R_{pim}	0.056 (0.62)	0.015 (0.073)
Reflections used in refinement	93,389 (9246)	33,600 (3327)
Reflections used for R-free	2095 (208)	1679 (167)
R_{work}	0.1525 (0.2912)	0.165
R_{free}	0.1936 (0.3453)	0.204
Macromolecules	3226	3212
Ligands	36	23
Solvent	454	246
Protein residues	410	410
RMS(bonds)	0.008	0.016
RMS(angles)	0.99	2.01
Ramachandran favored (%)	97.79	96.09
Ramachandran allowed (%)	2.21	3.67
Ramachandran outliers (%)	0.00	0.24
Average B-factor	26.28	20.39
Macromolecules	24.47	21.37
Ligands	15.88	18.32
Solvent	40.52	25.91

[a] The numbers in parenthesis refer to the highest resolution shell.

2.6. Low-volume differential scanning fluorimetry (nanoDSF)

The assay was carried out in 20 mM Hepes buffer pH 7.7, in the presence of 150 mM NaCl, with the protein concentration in the range 0.3–20 μM. The samples were loaded into nanoDSF grade Standard Capillaries (NanoTemper Technologies) and analyzed using the Prometheus NT.48 nanoDSF device (NanoTemper Technologies). Thermal unfolding of the protein was monitored using a linear thermal ramp (1 °C/min; 20–80 °C) with an excitation power of 30 %. The experimental data were analyzed with PR.ThermControl software. The middle-point temperature of thermal unfolding (T_m) was estimated based on the location of the maximum of the first derivative of the fluorescence intensity 350 nm/330 nm ratio.

2.7. Isothermal titration calorimetry

The isothermal titration calorimetry (ITC) measurements were done using a NanoITC calorimeter (TA Instruments). AdSS-His was dialysed against buffer, consisting of 20 mM Hepes, 50 mM NaCl, and 1 mM $MgCl_2$ with a pH value of 7.0. Ligands' solutions were prepared in the same buffer. All ITC measurements were conducted at 25 °C. The heat of ligand dilution was taken into account by performing a control titration reaction (buffer-ligand titration). Titration systems were designed as follows: titration of protein with GTP, titration of protein with IMP, titration of protein (previously incubated with IMP; final concentration 2 mM) with GTP, titration of protein (previously incubated with GTP; final concentration 2 mM) with IMP. In each titration system, the mixing rate was 250 rpm, AdSS concentration was 43 μM, and the concentration

of titrant (GTP or IMP) was 700 μM. Injection volume was 1.96 μL using a titration interval of 250 s for titration with GTP, 0.95 μL using a titration interval of 400 s for titration with GTP (enzyme pre-incubated with IMP), and 2.5 μL using titration interval of 400 s for titration with IMP (both cases).

NanoAnalyze software from TA Instruments was used to analyse the obtained data. Thermograms were constructed by subtracting the control titration, and all binding curves including the thermodynamic parameters were obtained using the One-Site fitting model.

2.8. Crystallization, data collection and structure determination

For fully ligated structure (AdSS-full), purified AdSS-His (15 mg/mL) was incubated with $MgCl_2$, GTP, IMP and hadacidin, Had (all ligands in 10× molar excess) for 30 min at room temperature. Crystallization trials were set up at 16 °C by the sitting-drop vapour diffusion method (volumes: 1 μL drop with 1:1 ration, 35 μL well) using Oryx8 Protein Crystallization Robot (Douglas instruments) and several commercial crystal screens: Morpheus I, II, III, ShotGun Eco I, Midas, JCSG+. Crystals appeared in several conditions in ShotGun Eco I screen after a few days. X-ray diffraction data collection from several crystals was done at the synchrotron beamlines P11 (PETRAIII, DESY, Hamburg) and Elettra (XRD2, Trieste). The data collection and refinement parameters for the best data set are summarized in Table 1. The data were processed using the XDS program [27]. The structure was solved by molecular replacement using the MOLREP program [28] and the structure of *Campylobacter jejuni* AdSS (PDB code 3R7T) as a search template. The model was refined using the phenix.refine routine from the PHENIX package [29]. Coordinates and structure factors have been deposited in Protein Data Bank under the accession number 6ZXQ.

Complex AdSS-IMP was obtained from crystallization of the purified protein (25 mg/mL) with $MgCl_2$, Asp, IMP and competitive inhibitor of GTP (in at least 10× molar excess of each ligand). The complex was incubated for 1 h at 4 °C. Crystals were obtained in conditions containing 0.1 M Bis-Tris Propane pH 8.35, 0.48 M ammonium sulphate and 27.7 % PEG 3350, at 12 °C by the hanging-drop vapour diffusion method (volumes: 4 μL drop, 600 μL well). Prior to flash-freezing in liquid nitrogen, crystals were soaked in a cryoprotectant solution containing 35 % polyethylene glycol (PEG) 3350. Data were collected on in-house diffractometer SuperNova (Oxford Diffraction/Rigaku) at 100 K using CuKα radiation wavelength (Table 1). Images were processed with CrysAlisPro software (Oxford Diffraction/Rigaku), and further analysis was performed with CCP4 [30]. The structure was solved by molecular replacement with PHASER [31], using *H. pylori* AdSS (UniProt code P56137) modelled on homologous *Bacillus anthracis* AdSS from SWISS-MODEL repository [32] as a model. Coordinates and structure factors have been deposited in Protein Data Bank under the accession number 7PVO.

2.9. Molecular dynamics simulations

The determined crystal structure of the *H. pylori* AdSS (6ZXQ) was used as the starting structure for preparing the systems subjected to computational simulations. Systems consisting of the wild type protein: (i) apo form of AdSS and its complexes with (ii) 6′-phosphoryl-inosine monophosphate (6-P-IMP), hadacidin (Had) and guanosine diphosphate (GDP), (iii) guanosine triphosphate (GTP), (iv) inosine monophosphate (IMP), (v) GTP and IMP. In addition, simulations were conducted for the protein with in silico introduced mutations in following complexes: (vi) AdSS(Q215A) with IMP, (vii) AdSS(Q215A) with GTP, (viii) AdSS (Q215A) with IMP and GTP, (ix) AdSS(S231A) with IMP, (x) AdSS (S231A) with GTP, (xi) AdSS(S231A) with IMP and GTP, (xii) AdSS (S231A/R135A) with IMP, (xiii) AdSS(S231A/R135A) with GTP, and (xiv) AdSS(S231A /R135A) with IMP and GTP.

Protonation of the protein was obtained with the H ++ server [33–35] so that the energy optimal H-bond network was achieved. Each

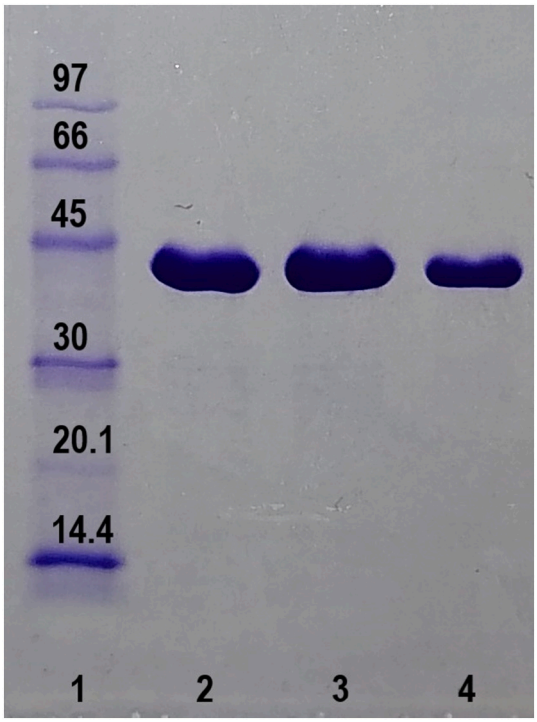

Fig. 1. SDS-PAGE of purified *H. pylori* AdSS-His. Lane 1 – LMW protein markers (molecular masses in kDa given in the figure), lanes 2–4 – purified AdSS-His (fractions from SEC column).

structure was placed in a truncated octahedron filled with a TIP3P model of water molecules. Sodium ions were added to ensure the electroneutrality of the system. Periodic boundary conditions (PBC) were applied. Protein atoms were parameterized using the ff14SB amber force field [36]. Ligands were parameterized using the GAFF force field [37,38]. Parameters for Na^+ and Mg^{2+} ions were taken from ff14SB amber force field [36,39]. In such a way, all 14 systems were prepared for computational simulations.

The geometry optimization (energy minimization) of each system was achieved in five cycles; each cycle consisted of 5000 steps. The steepest descent algorithm was used for the first 1000 steps, while the conjugate gradient algorithm was used for the remaining 4000 steps. In different cycles, harmonic potential with a force constant of 100 kJ mol^{-1} $Å^{-1}$ was applied to restrain different parts of the system. In the first cycle, enzyme and ligand atoms were restrained, while solvent molecules were relaxed. In the second cycle, the position of hydrogen atoms and solvent molecules were relaxed. In the third cycle, restrain was applied only on backbone atoms. The fourth optimization cycle had the same restraints as the previous, but with a force constant of 50 kJ mol^{-1} $Å^{-1}$. In the fifth cycle, there were no restraints.

Geometry optimised systems were subjected to the equilibration phase of molecular dynamics (MD) simulations which consisted of two stages. During the first stage which lasted 300 ps, the NVT ensemble was used, and the system was heated from 0 to 310 K. The temperature was linearly increased from 0 to 310 K during the first 250 ps and kept constant at 310 K for the next 50 ps using Langevin thermostat [40,41]. The second stage of equilibration phase lasted 200 ps, during which the NPT ensemble was used, the temperature was kept constant at 310 K using Langevin thermostat [40,41] and the pressure was kept constant at 1 atm using Berendsen barostat [42]. The integration step was 1 fs during the equilibration.

The production phase lasted 200 ns for each system, and the time step was 1 fs; Langevin's thermostat [40,41] and Berendsen's barostat [42] were applied. Statistical analyses of trajectories, such as calculations of RMSD, RMSF and changes in radius of gyration (Rg), were

Table 2
Distribution of AdSS-His, as a function of concentration, between monomeric and oligomeric forms, sedimentation coefficients, and molecular masses of these forms, obtained from analytical ultracentrifugation studies at pH 6.8–7.0, with or without 150 mM NaCl. Monomeric and dimeric forms may not sum up to 100 % as the addition of other forms is also observed (see Fig. 2).

Concentration of AdSS-His		pH	TCEP [mM]	NaCl [mM]	s	M	c(s) [%]	s	M	c(s) [%]
[μM]	[μg/ul]									
0.41	19	7	2	0	3.62	50.8	14.0	5.98	108	81.6
0.83	39				3.50	51.3	13.3	5.92	112	85.1
1.28	60				3.72	47.5	9.9	5.94	96	89.6
1.30	61	6.8	1	0	3.71	43.9	65.1	5.87	87	34.4
1.30	61			150	3.74	44.3	22.0	6.46	100	16.4[a]

[a] In the presence of 150 mM NaCl the higher oligomeric forms constitute >50 % of the sample.

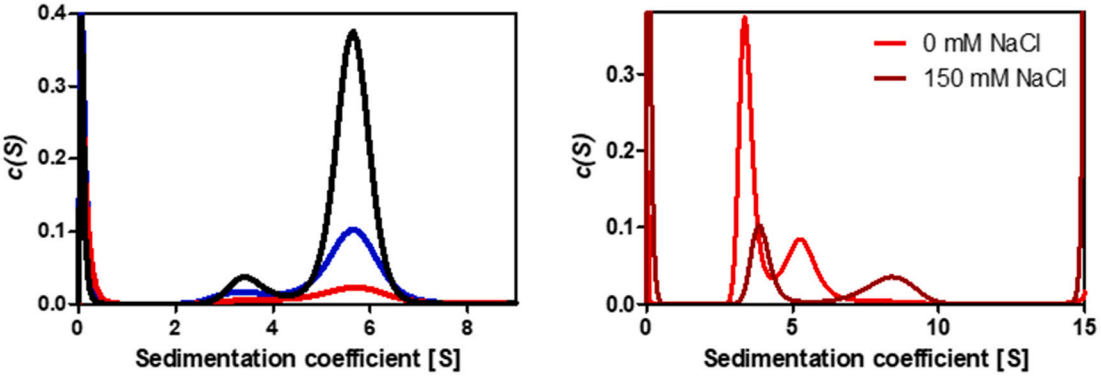

Fig. 2. Sedimentation coefficient distribution obtained for AdSS-His from *H. pylori* with the fitting range: 0–15 S. Left panel: c(S) distribution for three different protein concentration: 1.28 μM (black), 0.83 μM (blue), and 0.41 μM (red) in 20 mM Hepes buffer pH 7.0 + 2 mM TCEP. Right panel: c(S) distribution in 20 mM Hepes +1 mM TCEP with (dark red, pH 6.9, 1.50 μM AdSS) and without (light red, pH 6.8, 1.30 μM AdSS) 150 mM NaCl. AUC experiment was performed at 20 °C, 142,000 × *g*, and with absorbance detection at 225 nm.

performed using the CPPTRAJ module of AMBER16 software. Pymol (The PyMOL Molecular Graphics System, Version 2.0 Schrödinger, LLC) and VMD [43–47] were used for the visualization.

3. Results and discussion

3.1. Purification and properties of His-tagged H. pylori AdSS

Biophysical investigations generally require large amounts of pure enzyme, and researchers often accomplish this goal by attaching a sequence of 6 (or more) histidines (His-tag) to one of the protein's ends to facilitate protein purification on a metal ion-containing column (affinity chromatography). However, it has been proven that His-tag can sometimes affect an enzyme's structure and/or functionality (e.g. [48–50]). All reported investigations on bacterial adenylosuccinate synthetases were performed on native enzymes, i.e. with no tag attached [15]. As a simplified procedure for obtaining larger amount of the pure *H. pylori* AdSS was needed, the plasmid containing *purA* gene with His_6-tag attached at the protein's C-terminus (See Section 2.1) was prepared. This end of the sequence was chosen as it was known that the protein sequence of *E. coli* AdSS has a so-called P-loop, involved in the binding of GTP, close to the protein's N-terminus [16]. Therefore, insertion at the C-terminus is less likely to impact protein structure and/or function.

Table 3
The kinetic parameters for *H. pylori* AdSS-His, obtained by fitting the Michaelis–Menten equation to the experimental data. Fitting errors of the kinetic parameters obtained are shown in the table. Data for native AdSS are from reference [11].

	Variable substrate	Fixed substrates' concentration (mM)	K_M (μM)	V_{max} (U/mg)
AdSS-His	Asp	IMP-0.15, GTP- 0.06	176.3 ± 18.9	0.894 ± 0.030
	IMP	Asp-5, GTP-0.06	35.9 ± 4.6	0.956 ± 0.040
	GTP	Asp-5, IMP-0.15	15.6 ± 1.9	1.103 ± 0.040
Native AdSS	Asp	IMP-0.15, GTP- 0.06	125.4 ± 7.7	1.103 ± 0.016
	IMP	Asp-5, GTP-0.06	40.1 ± 2.9	1.456 ± 0.036
	GTP	Asp-5, IMP-0.15	8.7 ± 0.6	1.418 ± 0.023

The enzyme (AdSS-His) was purified through Ni-NTA and SEC columns (Fig. S1), to near homogeneity (as estimated by SDS-PAGE, Fig. 1). The shorter and simpler purification procedure (compared to purification of native enzyme [11]) gave significantly higher yield of purified enzyme for further analyses. Enzyme's monomer molecular weight (MW) was determined from SDS-PAGE to be 47.5 kDa, which correlates well with the theoretical MW of 46.8 kDa (as calculated by ProtParam) and is in range with MW of other characterized AdSSs [15]. Determination of the oligomeric state of AdSS-His on SEC gave somewhat ambiguous results. Namely, the MW calculated from elution volume was 76.1 kDa, between monomer and dimer. This could suggest the existence of a dynamic equilibrium between these two forms. Analytical ultracentrifugation (AUC) with the sedimentation velocity method was employed to check this hypothesis.

These experiments (Table 2 and Fig. 2), show that at pH 7.0 the majority of the sample (from 81.6 to 89.6 %, slightly dependent on protein concentration) constitutes a specie with a sedimentation coefficient $s^0_{20,w} \sim 5.9$ S and MW = 105.0 ± 9.0 kDa, hence corresponding to a dimer. The monomeric form constitutes a minority, 9.9–14.0 % of the sample. These results are comparable with those obtained for the AdSS wild type (WT), but at pH 6.8 [11]. At pH < 7.0, however, in contrast to the AdSS WT, the amount of the monomeric form of AdSS-His increases to >60 % (Table 2). The addition of 150 mM NaCl causes further change

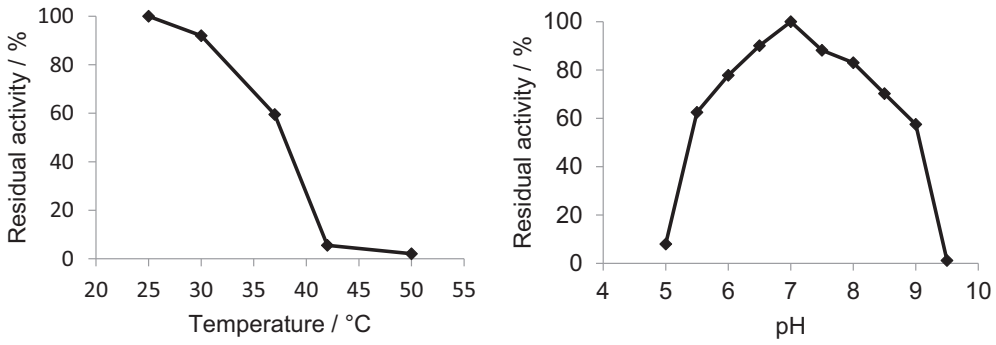

Fig. 3. Temperature (left) and pH (right) stability of *H. pylori* AdSS-His.

of the protein state, as monomers and dimers are present in comparable amounts, about 22 % and 16 %, respectively, but >50 % of the sample constitute higher oligomeric forms (Fig. 2 and Table 2). AUC results indicate that depending on pH and presence of NaCl, monomer and dimer, and in some conditions also higher oligomers, are indeed present in the AdSS-His samples, which explains why in SEC conducted at 20 mM Hepes buffer pH 7.0 containing 150 mM NaCl, MW between a monomeric and a dimeric form was observed.

To check whether this construct has an unchanged structure and function, regardless of its oligomeric distribution, it was characterized employing circular dichroism (CD) spectroscopy, kinetic measurements and thermal stability. CD spectra of native AdSS and AdSS-His were virtually identical (data not shown), indicating no changes in protein secondary structure. Kinetic constants for all three substrates are comparable to those of the native AdSS, as shown in Table 3. The stability range of AdSS-His is a bit narrower than for the native AdSS (Fig. 3), up to 30 °C and in the pH range 6.5–7.5, compared to 37 °C and the pH range 6.5–8.5 [11], respectively. Somewhat lower stability of AdSS-His was also detected through DSF measurements of melting temperature: T_m(AdSS-His) = 46.9 ± 0.3 °C and T_m(native AdSS) = 48.7 ± 0.2 °C.

As no significant effect of His-tag on AdSS function and secondary structure was observed, further experiments were performed with AdSS-His.

3.2. Binding of substrates and inhibitors to H. pylori AdSS

In a previous paper [11], AdSS inhibition constants for hadacidin (Had) and adenylosuccinate (AMPS) were determined to be 0.19 ± 0.02 μM and 3.5 ± 0.3 μM, respectively. Hadacidin is a natural antibiotic, produced by *Penicillium frequentans* [51], and it inhibits AdSS activity competitively towards Asp. Adenylosuccinate is the product of AdSS enzymatic reaction, and it inhibits the enzyme competitively towards IMP. During reaction catalysed by AdSS, GTP is hydrolysed to GDP, so the influence of GDP on *H. pylori* AdSS-His activity was investigated. As predicted, GDP had an inhibitory effect, competitive towards GTP (Fig. S2), with the inhibition constant of 0.84 ± 0.09 μM. It has been shown that AdSS enzymes are susceptible to product and feedback inhibition. As well as adenylosuccinate, GDP is a strong inhibitor with K_i in the range of 5–30 μM [15]. For example, for *E. coli* AdSS K_i(GDP) = 12 μM [25]. GDP inhibition constant for *H. pylori* AdSS-His is lower than cited values, indicating stronger inhibition (binding) of this enzyme with GDP.

To ascertain the affinity of *H. pylori* AdSS for each substrate, dissociation constants (K_d) for their interaction with AdSS-His were measured using isothermal titration calorimetry (ITC). Titrations of pure enzyme with IMP or GTP gave clear results, K_d(IMP) = 0.4 ± 0.1 μM and K_d(GTP) = 2.0 ± 0.8 μM (Fig. 4). However, when the enzyme pre-incubated with IMP was titrated with GTP (and vice versa), the titration curves became more complex, presumably due to the enzymatic reaction occurring (the transfer of the γ-phosphate from GTP to the 6-oxygen of IMP, forming the 6-phosphoryl IMP), and thus are not further discussed.

Binding of aspartate or hadacidin to AdSS-His in the absence of other substrates was not observed. It can reflect a genuine absence of binding, or it can be due to a much too small difference in heat energy to be measured by this method in given conditions. However, the absence of binding of Asp/Had to apo-protein would be in line with the proposed molecular mechanism of catalysis [52]. In the first step, the γ-phosphate from GTP is transferred to the 6-oxygen of IMP, thus forming the intermediate 6-phosphoryl IMP (6-P-IMP). Only afterwards is the 6-phosphoryl group displaced by the α-amino group of aspartate to form adenylosuccinate (AMPS).

The data on dissociation constants of other AdSS enzymes are scarce. Only the data on *E. coli* AdSS is available, obtained from fluorescence measurements [53]. For this enzyme, measured dissociation constants are in the micromolar range: K_d(IMP) = 37.7 μM, K_d(GTP) = 23.7 μM, K_d(AMP) = 148 μM, and K_d(AMPS) = 1.8 μM [53], essentially in the same range as corresponding K_M and K_i values for this enzyme [15]. Here presented results show at least 10-fold lower K_d values, compared to respective K_M values, for IMP and GTP (compare Table 3 and Fig. 4). Although dissociation constants are often approximated with Michaelis constants, one should keep in mind that these two constants have inherently different meanings (the first is a thermodynamic parameter, and the second is a kinetic parameter). Also, in a complex three-substrate system, like AdSS, the assumptions needed for K_M to approximate K_d are numerous and difficult to fulfill [54].

3.3. Overall structure of His-tagged H. pylori AdSS — fully ligated structure (AdSS-full)

Out of 419 amino acids present in the protein sequence (411 of native protein +2 linker amino acids +6 His), 412 are observed in the electron density. N-terminal Met is missing, as well as the affinity tag (6 His). Processing of N-terminal Met is common, especially if the following amino acid is small (Ala in *H. pylori* AdSS), although it can sometimes be omitted during recombinant protein expression [55]. The affinity tag is most likely too flexible to be observed. The affinity tag on the C-terminal end of the protein is positioned at the opposite side of the active site, making it not likely to affect the properties of *H. pylori* AdSS (Fig. 5).

The overall enzyme structure is similar to those of other AdSS enzymes (Fig. 5), with the highest level of structural similarity to the structures of AdSSs from *E. coli* (EcAdSS, PDB code 1CG0 [19], sequence identity 46 %) and *Plasmodium falciparum* (PfAdSS, PDB code 1P9B [20], sequence identity 40 %), that have the same set of ligands enclosed in the active site. The conformationally invariant core comprises a β-sheet of 9 β-strands (8 mutually parallel and one anti-parallel). Individual strands are connected via various structural elements – loops, helices, strands, and combinations of those (Fig. 5). The RMSD (root-mean-square deviation) difference in alignment is 1.09 and 1.21 with EcAdSS and PfAdSS, respectively, as calculated with PDBeFold [56]. Apart from

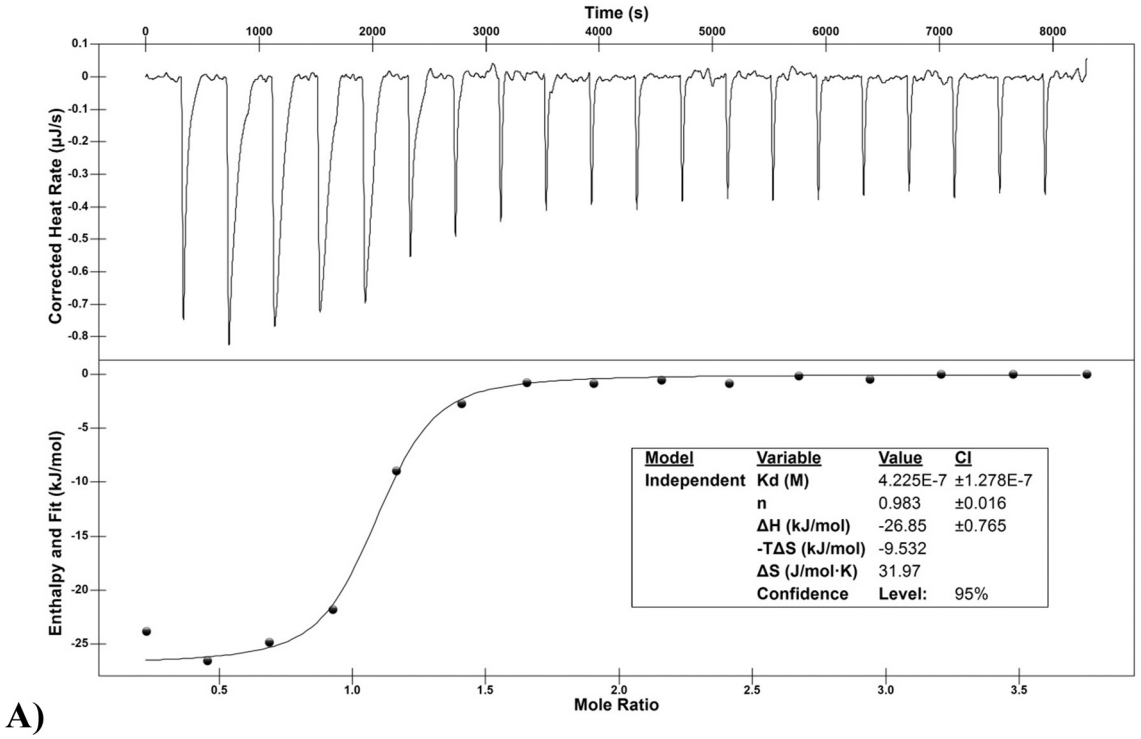

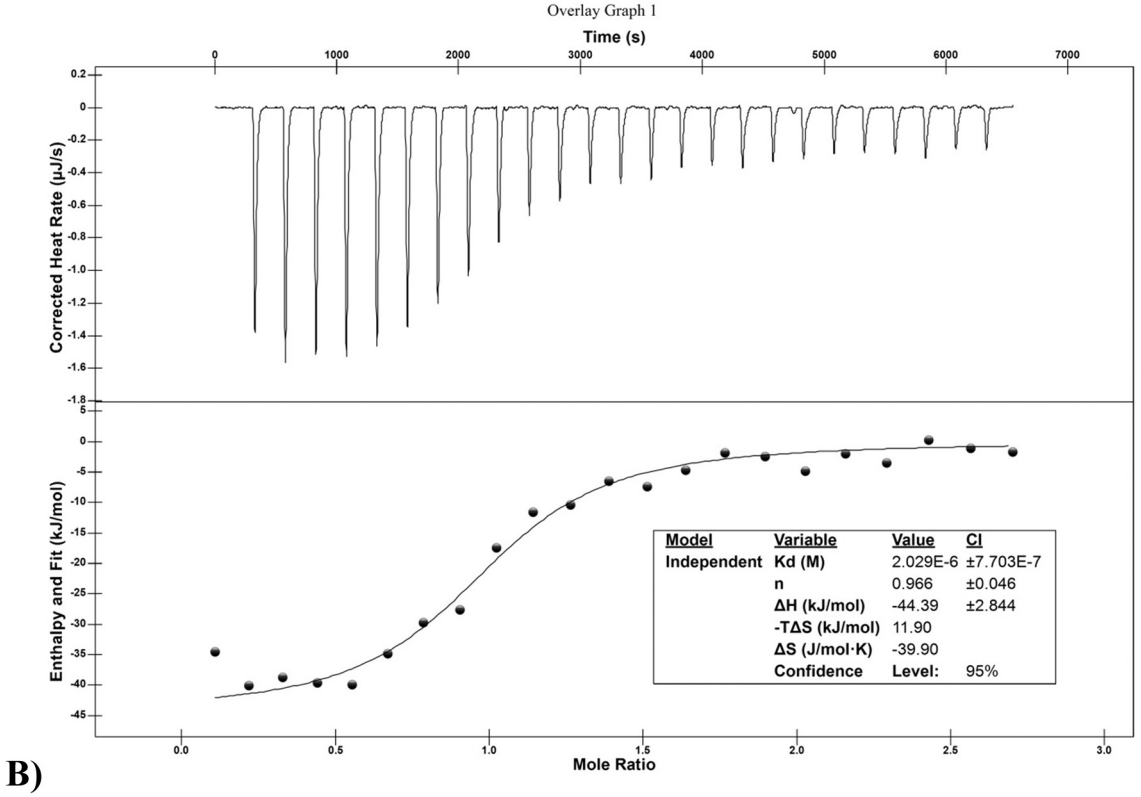

Fig. 4. Binding of substrates to *H. pylori* AdSS-His, as characterized by ITC. Binding of A) IMP and B) GTP with Mg^{2+} present in the solution. Dissociation constants (K_d) and thermodynamical parameters are shown in the box.

minor differences in the secondary structure elements, the structures are practically identical in the active site area (ligands and loops in contact with them align perfectly).

The buried surface area between monomers in the structure of EcAdSS is 2745.4 Å^2, which is considerably larger than either that of *H. pylori* AdSS or PfAdSS (2342.4 and 2392.2 Å^2), as calculated by PDBePISA [57]. Along with that, there is a much larger number of hydrogen bonds on the interface area in EcAdSS than in *H. pylori* AdSS (HpAdSS) or PfAdSS (50 compared to 28 and 30). This suggests tighter dimer binding of EcAdSS than HpAdSS or PfAdSS. Also, a substantial

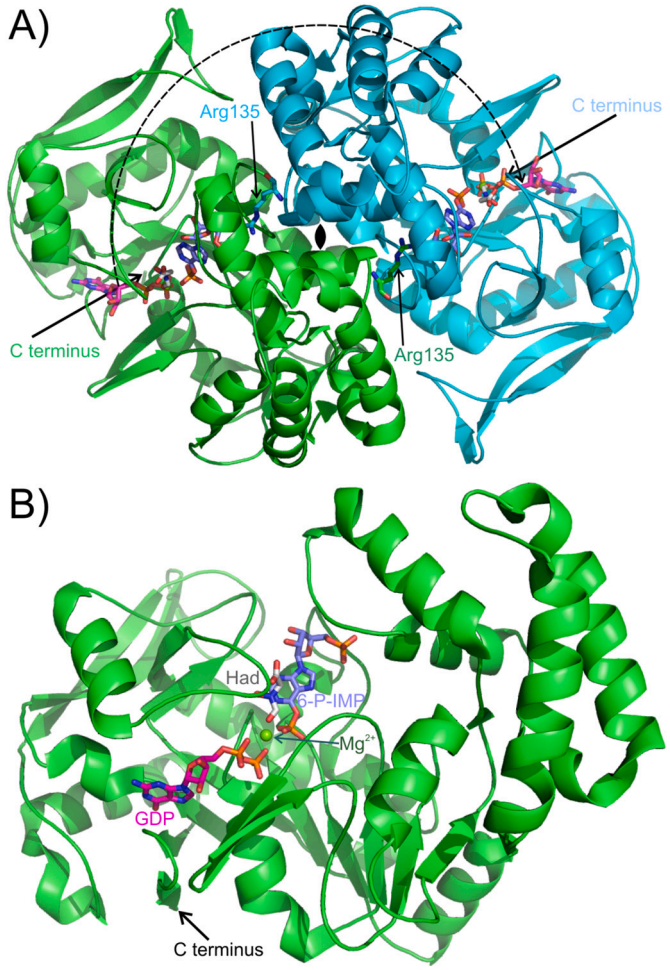

Fig. 5. The overall structure of *H. pylori* AdSS. A) Two identical monomers (shown in green and teal) of *H. pylori* AdSS join to form a dimer over a two-fold symmetry axis (denoted in the centre, and by the dashed line). The active sites are positioned on the opposite sides of the monomer-monomer interface. Amino acid Arg135 from each monomer completes the active site of the other. C-termini of both monomers, where the histidine tag is attached but not visible in the structure, are located on the protein's surface on the bottom side. B) The top-down view of the active site of one of the monomers with the positions of bound ligands.

number of hydrogen bonds is found between amino acids which are on equivalent positions in multiple sequence alignment: 18 between HpAdSS and PfAdSS; 14 between HpAdSS and EcAdSS; and 14 between PfAdSS and EcAdSS. Of these conserved hydrogen bonds, 12 are common to all three structures. All of them are between the 135–139 loop region from one monomer and the 222–232 region from the other monomer. This is also where the amino acid Arg135 participates in completing the active site of the neighbouring monomer, and probably reflects the importance of the positioning of these loops.

The asymmetric unit contains one molecule of *H. pylori* AdSS; however (similar to other AdSS enzymes) we observed that Arg135 from one monomer participates in the active site of the neighbouring subunit (in the binding of IMP), thus indicating the necessity of dimer formation for the formation of the functionally capable enzyme (Fig. 5A).

3.4. Interactions in the H. pylori AdSS active site - crystal structure AdSS-full

Each monomer of the AdSS dimer contains one active site. The active site is a wide shallow pocket parallel to the protein surface as it has to accommodate three substrates and a magnesium ion. Instead of IMP and GTP added to the enzyme during crystallization, 6-phosphoryl-IMP (6-P-IMP) and GDP are observed in the active site (Fig. 6). As already mentioned, according to the generally accepted AdSS mechanism [52], the first step of the reaction is the formation of 6-phosphoryl-IMP by nucleophilic attack of the 6-oxo group of IMP on the γ-phosphorus atom of GTP, which is then followed by the nucleophilic displacement of the 6-phosphoryl group by L-aspartate to form adenylosuccinate. As in this structure hadacidin (Had) is present instead of L-aspartate (Asp), the reaction cannot proceed so 6-P-IMP, GDP and Had are trapped in the active site.

The Mg^{2+} is located in the centre of the active site. It connects all the substrates, as it is octahedrally coordinated by 6 oxygen atoms from: the *N*-formyl group of hadacidin, the 6-phosphoryl group of 6-P-IMP, the α- and β-phosphoryl groups of GDP, the backbone carbonyl group of Gly39 and the side-chain carbonyl group of Asp12 (see Fig. 7A). Indeed, Honzatko and coworkers [16] concluded that the coordination of Mg^{2+} in the active site is probably the central factor in forming the catalytically productive complex.

6-P-IMP realizes numerous interactions within its part of the active site (Fig. 7). The α-phosphoryl group makes hydrogen bonds with side chains of Arg*135 (from the adjacent monomer), with Asn37 and Thr121, as well as with the main chain groups of Thr230 and Thr121. Sugar moiety interacts with the side chain of Arg294 and with the main chain groups of Val264 and Gly119. Finally, the 6-phosphoryl group forms as many as 10 hydrogen and electrostatic bonds, with: side chains of His40, Lys15, Asp12 and Gln215, main chain groups of Gly39, Asp12 and Gln215, as well as with the β-phosphoryl group of GDP, *N*-formyl group of hadacidin and Mg^{2+} ion.

Similar to 6-P-IMP, charged molecule of GDP also requires a plethora of interactions for its stabilization within the enzyme's active site (Fig. 7). The purine base part of GDP makes hydrogen bonds with Ser400 and Asp334, and the carbonyl group on the base interacts with main chain groups of residues 400–402. Sugar part of GDP hydrogen bonds to the side chain of Lys322. The α-phosphoryl group makes hydrogen bonds with side chains of Thr41, Thr290, Arg296 and Asp12. Additionally, it interacts with the Mg^{2+} ion and the *N*-formyl group of hadacidin. β-Phosphoryl group of GDP makes hydrogen bonds with the side chain of Lys15 and main chain groups of residues 13–16. Also, it interacts with the Mg^{2+} ion and the oxygen atom from the 6-phosphoryl group of 6-P-IMP.

The *N*-formyl group of hadacidin is bound to Mg^{2+} ion, oxygen atom from the β-phosphoryl group of GDP and oxygen atom from the 6-phosphoryl group of 6-P-IMP, as well as with the side chain of Asp12. The carboxyl group makes hydrogen bonds with side chains of Arg294 and Thr292, as well as with the main chain groups of residues 291–292. Hydroxyl group hydrogen binds to side chains of Arg296 and Asp12.

It is clear that packing in the active site is tight, as there are many residues that interact with more than one ligand, i.e. Asp12 binds Mg^{2+} and all three ligands, residues 290–296 are involved in interactions with all three ligands, Gly39 binds Mg^{2+} and 6-P-IMP. Also, as already mentioned, Mg^{2+} is coordinated by all three ligands, and the ligands are all inter-connected.

As in the case of *E. coli* AdSS, one residue from the adjacent monomer protrudes to the active site and participates in the binding of IMP (or 6-P-IMP) – Arg*135 (Arg143 in *E. coli* AdSS). Even though the active site faces the opposite side of the monomer-monomer interface, the position of this Arg residue is apparently unaffected by the presence of ligands in the *E. coli* enzyme. Mutation of this residue to Leu does not diminish the enzyme's catalytic efficiency, however it significantly increases K_M constants for GTP and especially IMP, thus indicating this residue as critical in the binding of substrates in the active site of *E. coli* AdSS [58].

3.5. Interactions in the H. pylori AdSS active site — molecular dynamics simulations

Molecular dynamics (MD) simulations enabled the study of the

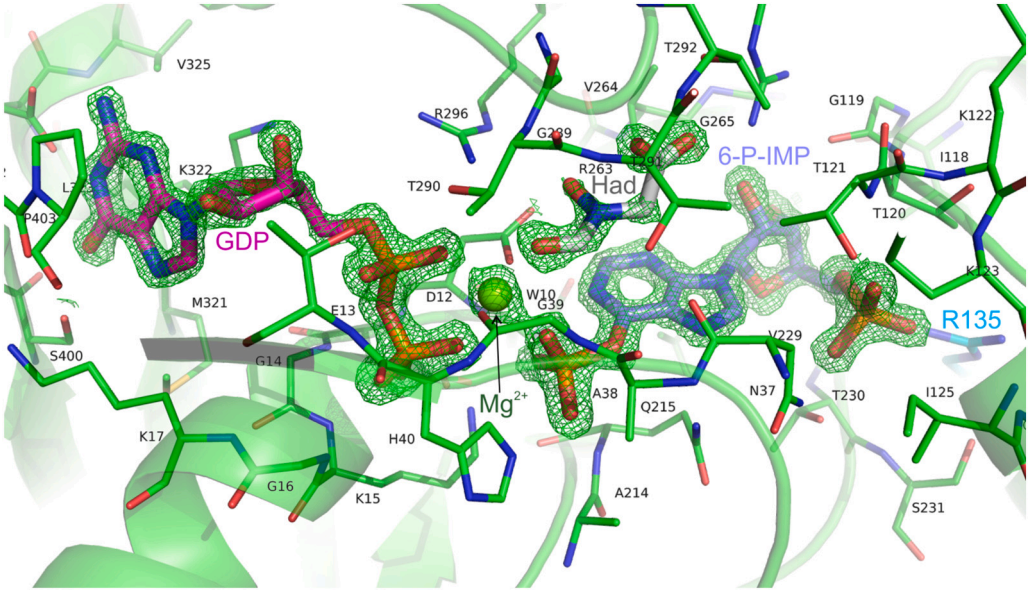

Fig. 6. The 2*mFo-DFc* difference electron density map contoured at 1σ level around ligands in the active site of *H. pylori* AdSS. The electron density is of excellent quality at 1.4 Å resolution, and all parts of molecules are clearly defined. This is due to the very tight funnel shape of the active site. Arg135 from the neighbouring monomer is visible on the far right.

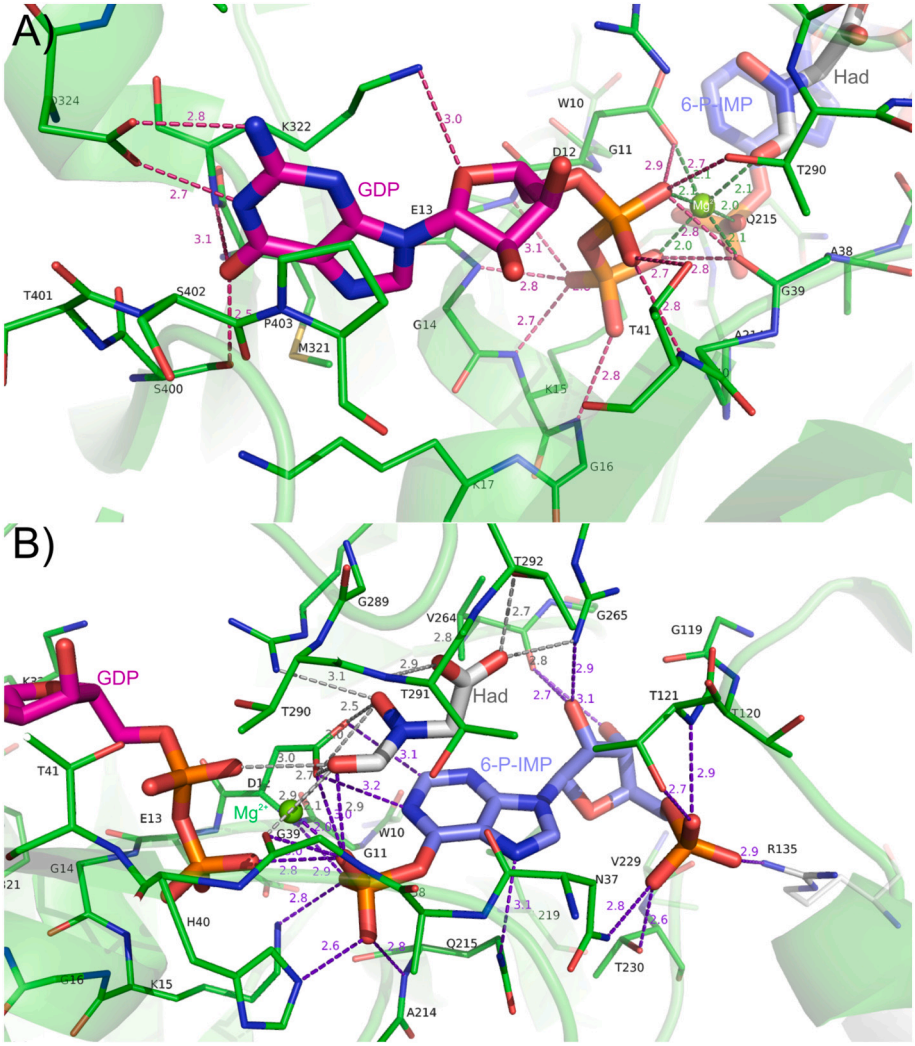

Fig. 7. Interactions of ligands in the active site of *H. pylori* AdSS. Hydrogen bonds and polar contacts shorter than 3.2 Å are shown and coloured with the colour of the corresponding ligand. Water molecules are omitted for clarity. The green sphere is an Mg^{2+} ion. A) GDP molecule is bound with the purine plane oriented by hydrophobic interactions with Pro403, Met321 and Lys322, while it makes a large number of hydrogen bonds with surrounding residues. The diphosphate group is also very tightly coordinated with almost every oxygen atom making polar contacts with amino acids around it or with the Mg^{2+} ion, which is coordinated by all three ligands and occupies the central position in the active site. B) Molecule of 6-P-IMP is also coordinated with many hydrogen bonds and polar contacts. It is oriented with its PO_4 group at position 6 towards the Mg^{2+} ion. The hydrogen bond contact with Arg135 from the neighbouring chain is visible on the opposite end to the far right.

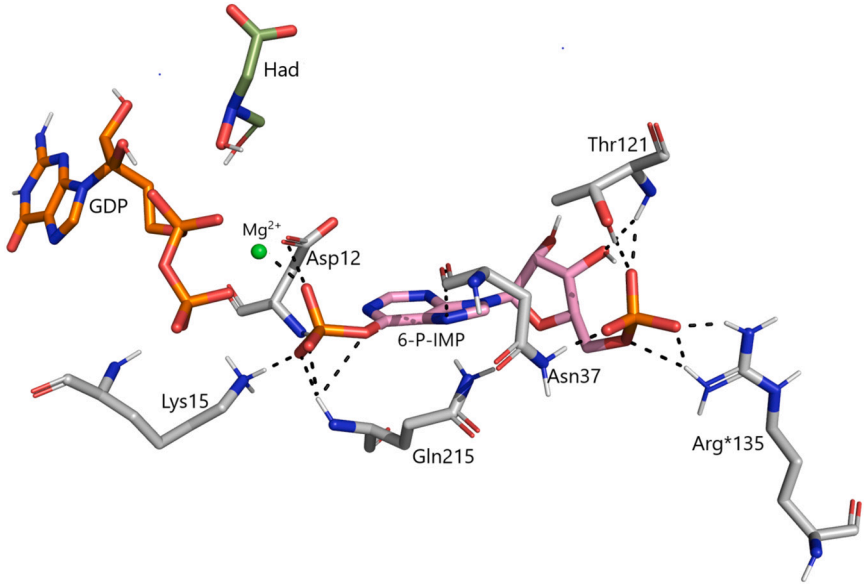

Fig. 8. Stabilization of 6-P-IMP 6′-phosphate via preserved H-bond interactions in the active site of *H. pylori* AdSS. Hydrogen bonds that stabilise Had and GDP are omitted for clarity.

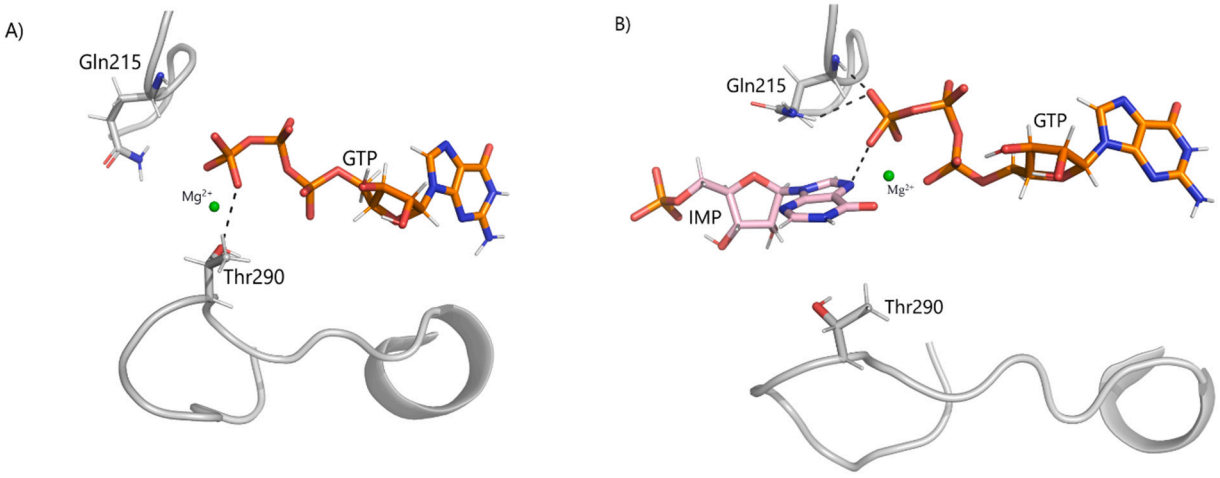

Fig. 9. GTP conformation and its stabilization via Thr290 in the A) absence and B) presence of IMP in the active site of *H. pylori* AdSS.

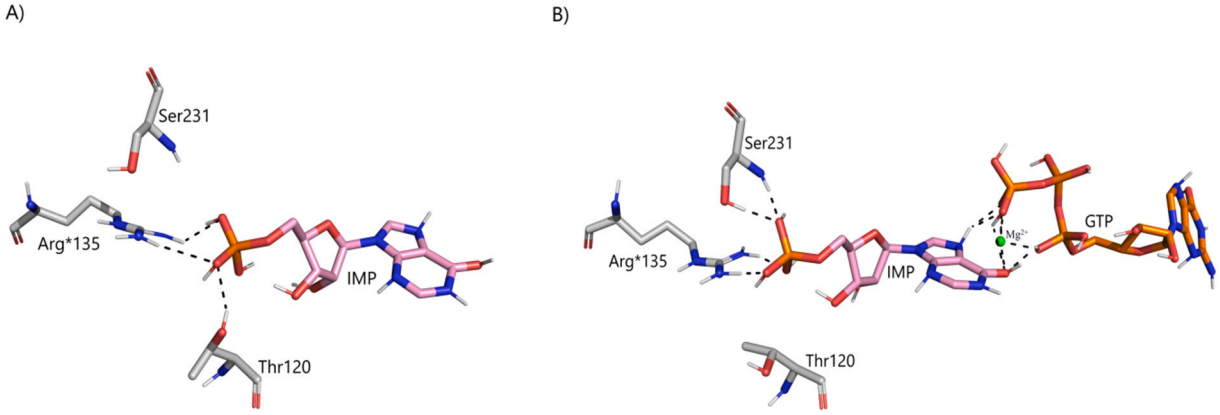

Fig. 10. IMP conformation and its stabilization in the A) absence and B) presence of GTP in the active site of *H. pylori* AdSS.

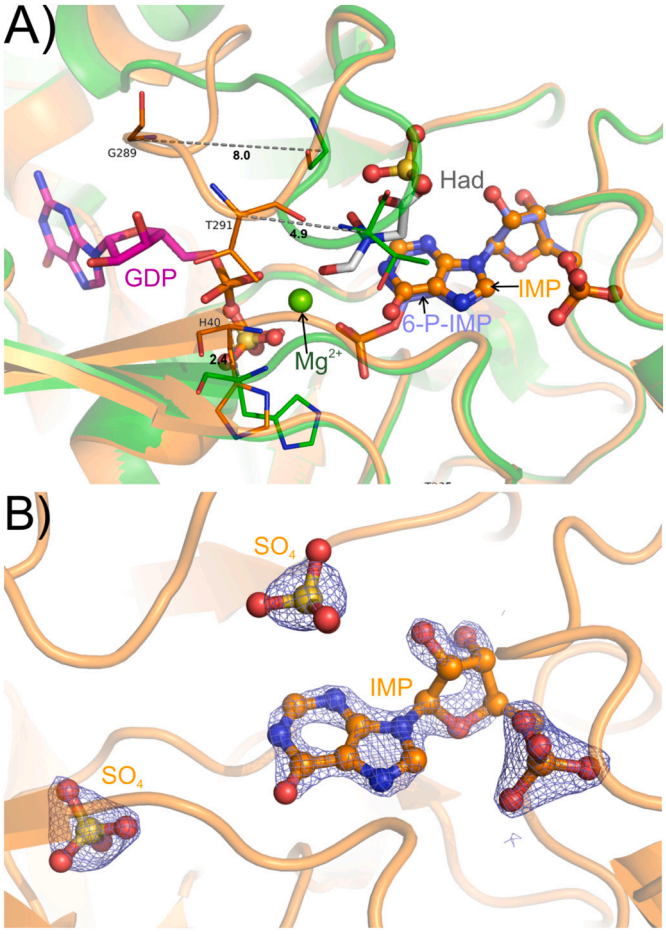

Fig. 11. Comparison of active sites of AdSS-full (colouring as on Fig. 5) and AdSS-IMP (orange). A) Two major differences in the active site conformation are shown; distances are measured between Cα atoms of the same amino acids in both structures: His40 (2.4 Å), Gly289 (8.0 Å), Thr291 (4.9 Å). Since there is no GDP molecule, the loop can move to occupy its place. The position of IMP and 6-P-IMP is almost completely identical. B) 2*mFo-DFc* electron density contoured at 1σ level depicted around IMP molecule in the structure of AdSS-IMP in the same orientation as on panel A. Two additional molecules of SO_4 are fitted in the electron density; one is bound in the position of the terminal PO_4 of GDP and the other roughly to the end of the hadacidin molecule.

dynamical properties of the protein, especially of the active site, and the durability of non-covalent interactions identified by the X-ray diffraction. Simulations showed persistent stabilization of GDP binding through H-bonds with Ser400, Lys15, Gly14, His40, and Gly16, as well as through electrostatic interactions with Mg^{2+} (Fig. S3. – Fig. S7. in the Supplement). The 6-P-IMP 6′-phosphate stabilization via H-bonds with the Lys15, Gln215, Asn37, and Asp12 was also preserved during the simulations (Fig. 8). The most significant contribution to positioning and stabilizing the 6-P-IMP is the H-bond via the side chain of Arg135 from the other monomer (Arg*135), which is preserved during all simulations.

Simulations of systems with substrates show that presence of both IMP and GTP helps their mutual positioning into positions suitable for the transfer of the GTP γ-phosphate group to the 6′-oxygen of IMP (Fig. 9B). During the simulations of the GTP-enzyme system without IMP presence, GTP is in a less extended conformation and its γ-phosphate group is stabilized by interactions with Thr290 (Fig. 9A). Simulations of the enzyme-GTP system in the presence of IMP show that GTP adopts an extended conformation, and its γ-phosphate group is stabilized via H-bonds with IMP and Gln215 (Fig. 9B). In other AdSS enzymes with solved structure, in a position analogous to position 215 of *H. pylori* AdSS, there is Gln or Asn residue, indicating the importance of the COOH group in the stabilization of γ-phosphate group of GTP (Fig. S8). However, Thr is not conserved in a position analogous to position 290 of *H. pylori* AdSS (Ala in *E. coli* AdSS, Val in mouse and human AdSS, Fig. S8).

At the same time, the presence of GTP affects the positioning of IMP. During MD simulations of IMP-enzyme without GTP (Fig. 10A), IMP is stabilized by H-bonds with Thr120 and Arg135 from another monomer (Arg*135). During MD simulations of IMP-enzyme in the presence of GTP (Fig. 10B), repositioning of IMP occurs, and stabilization is achieved through H-bonds with Arg*135 and Ser231. Furthermore, IMP is stabilized by electrostatic interactions via magnesium ion and the γ-phosphate group of GTP. MD simulations of Ser231Ala mutant and Ser231Ala/Arg135Ala double mutant show that IMP stabilization by interaction with Arg*135 is significantly more important than stabilization by interactions with Ser231. All mentioned residues are conserved in AdSS enzymes (Fig. S8).

3.6. Comparison of AdSS-full with a structure comprising only IMP in the active site (AdSS-IMP)

In preparation of crystallization sample that lead to AdSS-full structure, enzyme was incubated with its substrates and one of the substrates was replaced with its analogous inhibitor – Asp with Had. Replacing the GTP with the analogue of GTP in the incubation mixture prior to crystallization was also tried. However, even though the enzyme was incubated with aspartate, IMP, GTP analogue and Mg^{2+} ions, only IMP was observed in the AdSS-IMP structure. Positions of the purine base, sugar moiety and α-phosphoryl group are virtually the same in both complexes, and the hydrogen bonds network is almost the same (Fig. 11). α-Phosphoryl group of IMP interacts with Arg*135 from the other subunit of the dimer and with Thr221; sugar forms bonds with Gly119 and Val264, purine base with Gln215. In the case of IMP bound in the AdSS-IMP complex, oxygen atom O6 forms the hydrogen bond with the side chain of Asn37, whereas O6 from 6-P-IMP binds with the side chain of Gln215, as the purine ring is slightly tilted (10°). There are slight differences in the secondary structure between fully ligated protein and the AdSS-IMP complex (Fig. 11). The loop 287–293 is moved away from the active site about 8 Å, and is poorly visible in the electron density, which is likely related to the lack of Asp or its analogues in the crystallized complex [59]. Also, the N-terminus of β-strand 40–44 and Gly39 are moved about 2.4 Å towards the protein surface vs. the same region in the AdSS-full structure. This region interacts with Mg^{2+} ion (Gly39) and α- and β-phosphoryl groups of GDP which are not bound in the AdSS-IMP complex. Both regions are conserved in other AdSS enzymes, as they are involved in binding of substrates (Fig. S8).

Differences between fully ligated and IMP complex for *H. pylori* AdSS are similar to those for *E. coli* AdSS, structures 1CG0 [19] and 1KJX [59], respectively. The similarity between structures 6ZXQ and 1CG0 (RMSD 0.61, as calculated by *align* in PyMOL), as well as IMP-complex and 1KJX (RMSD 0.81, as calculated by *align* in PyMOL) suggests that in the case of *H. pylori* AdSS, similar like for *E. coli* AdSS, binding of IMP alone organizes most of the active site, and Arg135 plays the same role in forming and stabilizing dimeric form, as Arg143 in *E. coli* AdSS [59].

Even though the structure of the apo form of *H. pylori* AdSS is not available, above-mentioned similarities between *H. pylori* AdSS and *E. coli* AdSS structures allow the assumption that in the apo form *H. pylori* AdSS most probably has a disorganized active site, similarly to *E. coli* AdSS.

3.7. Flexible elements of H. pylori AdSS structure

A high level of congruence between our structures and analogous *E. coli* AdSS structures (1CG0 and 1KJX) encouraged comparison of AdSS-full structure to the unligated *E. coli* AdSS structure (1ADE, [60]). The overall RMSD for this overlap is 1.87 Å (as calculated by *align* in

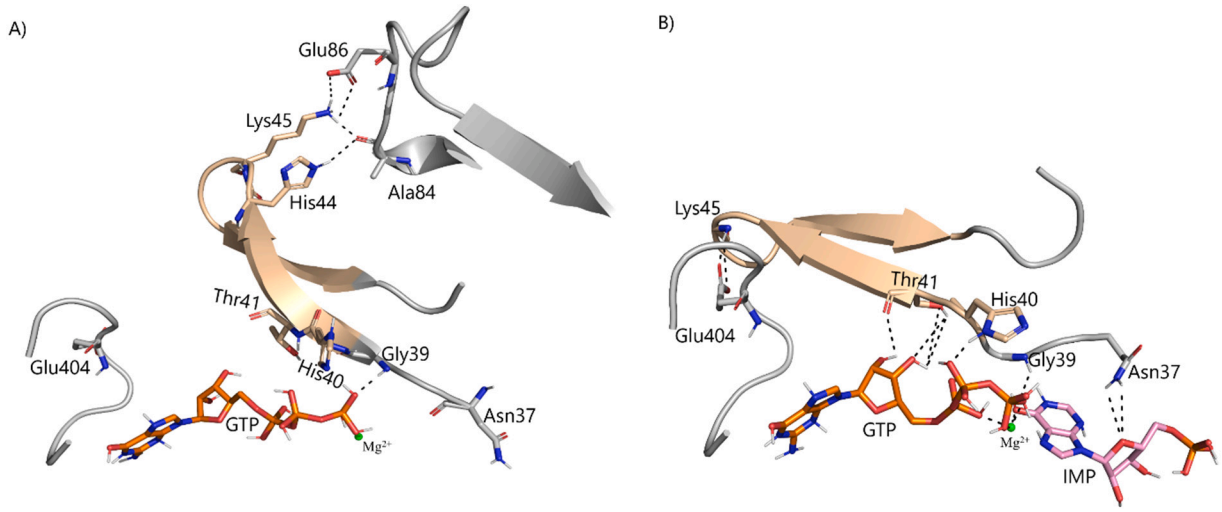

Fig. 12. GTP-binding loop conformation: A) in the presence of only GTP in the active site of *H. pylori* AdSS, B) closed conformation in the presence of IMP and GTP. Hydrogen bonds that stabilise the open or closed conformation of the GTP-binding loop in *H. pylori* AdSS are shown as dashed lines.

PyMOL), however regions of pronounced conformational changes could be identified. The most significant changes involve residues 36–53 and 275–296, which is in agreement with the results obtained by MD simulations (see later), as well as the comparison of AdSS-full and AdSS-IMP structures (see Section 3.6.). Region 36–53 comprises two anti-parallel β-strands with a short loop between them. The beginning of this region is involved in binding of GDP (see Section 3.5.). Region 275–295 contains one α-helix (H12) followed by a loop (residues 285–295). This loop is involved in interactions with all three ligands (except Mg^{2+} ion) in the active site (see Section 3.4).

In order to get better insight into conformational changes in *H. pylori* AdSS that occur upon substrate binding, molecular dynamics simulations were employed. Simulations of the enzyme-GTP and enzyme-IMP-GTP systems showed the conformational change of the GTP binding loop consisting of amino acids 40–50 that does not occur during the simulations of the systems lacking the IMP in the active site (Fig. 12). The mean value of RMSF (root mean square fluctuation) for the GTP binding loop is 2.42 ± 1.36 Å in the absence of IMP in the active site, while this value is 1.23 ± 0.56 Å during the simulations with IMP present in the AdSS active site (Fig. S9). Involvement of the loop consisting of amino acids 40–50 in the conformational change is in accordance with our X-ray results (see Section 3.6).

Conformational change of the active site induced by the IMP was already known from the literature [59], while analyses of MD simulations enabled understanding of its molecular basis. The presence of IMP in the active site causes the formation of an H-bond network starting from Asn37 and proceeding towards the enzyme's C-terminus, leading to a closed conformation of the GTP-binding loop (Fig. 12B). Such H-bond network consists of amino acids: Asn37 which forms an H-bond with the ribose part of the IMP, Gly39 which forms an H-bond via the protein backbone with the 6′-oxygen atom of IMP, and His40 which forms a hydrogen bond with the β-phosphate group of GTP, while Thr41 interacts with hydroxyl 2′ and 3′ groups of the GTP ribose. The H-bonds between Lys45 and Glu404 further stabilise the closed conformation of the loop. The importance of Asn37, starting amino acid of the described H-bond network, for the AdSS catalytic mechanism is supported by the kinetic experiments on the *E. coli* AdSS involving the wild type and the Asn38Ala mutant (analogous position to Asn37 in *H. pylori* AdSS) [59,61]. Without the presence of IMP, a different H-bond network was observed, formed by His44, Ala84, Lys45, and Glu86 (Fig. 12A).

4. Conclusion

The results presented in this paper show the properties of the first bacterial adenylosuccinate synthetase (AdSS from *Helicobacter pylori*) purified with a histidine tag. They indicate that even though the oligomeric distribution is different in the tagged enzyme compared to the native one, the structure and catalytic properties are not significantly altered by the His_6-tag. Comparison of interactions in the active site in both solved X-ray structures (AdSS-full, with 6-P-IMP, GDP, Had and Mg; and AdSS-IMP, with IMP and two sulphate ions) and molecular dynamics simulations allowed for the identification of the most persistent ones. Particularly, the H-bond between IMP's α-phosphate and the side chain of Arg*135 (from the adjacent monomer) proves to be of paramount importance for dimerization of enzyme and formation of the active site. IMP was shown to be responsible for the organization of most of the active site, however loops comprising residues 287–293 and 40–44 occupy different positions in structures AdSS-full and AdSS-IMP. The former loop participates in binding of Had (or Asp) and the latter in binding of GDP (or GTP). Molecular dynamics simulations identified the network of H-bonds that keeps a loop made of residues 40–50 in the closed conformation. That network is formed only in the presence of IMP and it puts GTP in the position favourable for the reaction to occur, thus suggesting the synergistic effect of substrates (IMP and GTP) binding in the active site.

Recent research on inhibition of the adenylosuccinate synthetase is mainly directed either towards the treatment of e.g. cancers (e.g. [62]), or towards the herbicidal activity of new derivatives of hydantoin (e.g. [63]). Inhibitory effect on AdSS enzymes was shown for potentially antifungal [64] and antimalarial compounds [65]. However, data on the potential of AdSS inhibitors as antibacterial drugs is scarce. In this light, described results present a solid basis for the design of better inhibitors of *H. pylori* AdSS, which could lead to new antibiotics for eradication of this dangerous pathogen.

CRediT authorship contribution statement

Ante Bubić: Investigation, Visualization, Writing – original draft. **Marta Narczyk:** Investigation, Supervision, Writing – original draft. **Ana Petek:** Investigation. **Marta Ilona Wojtyś:** Investigation. **Weronika Maksymiuk:** Investigation. **Beata Wielgus-Kutrowska:** Investigation. **Maria Winiewska-Szajewska:** Supervision. **Tea Pavkov-Keller:** Investigation, Supervision, Writing – review & editing. **Branimir Bertoša:** Validation, Supervision, Writing – original draft, Writing –

review & editing. **Zoran Štefanić:** Validation, Visualization, Writing – review & editing, Project administration, Funding acquisition. **Marija Luić:** Conceptualization, Supervision, Writing – review & editing, Project administration, Funding acquisition. **Agnieszka Bzowska:** Conceptualization, Methodology, Validation, Supervision, Writing – original draft, Writing – review & editing, Project administration, Funding acquisition. **Ivana Leščić Ašler:** Methodology, Investigation, Validation, Supervision, Writing – original draft, Writing – review & editing.

Declaration of competing interest

The authors declare that they have no known competing financial interests or personal relationships that could have appeared to influence the work reported in this paper.

Acknowledgements

Experiments conducted in Croatia were financed by Croatian Science Foundation (projects no. IP-2013-11-7423 and IP-2019-04-6764). CD spectroscopy measurements were performed in Laboratory for Biomolecular Interactions and Spectroscopy, Ruđer Bošković Institute. The research stay of A. Bubić in Graz was financed by Go-Styria scholarship. A. Bubić is thankful to dr. Nives Ivić who helped with the construction of *pET21b-HPpurA-His* plasmid. Experiments conducted in Poland were financed by the project Harmonia 2015/18/M/NZ1/00776 granted by the National Science Centre of Poland, from the University of Warsaw project IDUB PSP-501-D111-20-0004316, and by the Polish Ministry for Science and Higher Education grant 501-D111-01-1110102. Analytical ultracentrifugation was conducted in the NanoFun laboratories, ERDF Project POIG.02.02.00–00-025/09. X-ray studies and some other experiments were performed in the Laboratory of Biopolymers, ERDF Project POIG.02.01.00–14-122/09. We acknowledge DESY (P11 beamline, PETRAIII, Hamburg, Germany) and Elettra (XRD2, Trieste) for provision of synchrotron-radiation facilities and support during data collection.

Appendix A. Supplementary data

Supplementary data to this article can be found online at https://doi.org/10.1016/j.ijbiomac.2022.12.001.

References

[1] B. Linz, F. Balloux, Y. Moodley, A. Manica, H. Liu, P. Roumagnac, D. Falush, C. Stamer, F. Prugnolle, S.W. van der Merwe, Y. Yamaoka, D.Y. Graham, E. Perez-Trallero, T. Wadstrom, S. Suerbaum, M. Achtman, An african origin for the intimate association between humans and helicobacter pylori, Nature 445 (2007) 915–918, https://doi.org/10.1038/nature05562.

[2] B.J. Marshall, J.R. Warren, Unidentified curved bacilli in the stomach of patients with gastritis and peptic ulceration, Lancet 1 (1984) 1311–1315, https://doi.org/10.1016/S0140-6736(84)91816-6.

[3] M. Miftahussurur, Y. Yamaoka, D.Y. Graham, Helicobacter pylori as an oncogenic pathogen, revisited, expert. Rev, Mol. Med. 19 (2017) 1–11, https://doi.org/10.1017/erm.2017.4.

[4] K. Robinson, J.C. Atherton, The spectrum of helicobacter-mediated diseases, Annu. Rev. Pathol. Mech. Dis. 16 (2021) 123–144, https://doi.org/10.1146/annurev-pathol-032520-024949.

[5] J. Jessurun, Helicobacter pylori: an evolutionary perspective, Histopathology 78 (2021) 39–47, https://doi.org/10.1111/his.14245.

[6] S. Ansari, Y. Yamaoka, Survival of helicobacter pylori in gastric acidic territory, Helicobacter 22 (2017), e12386, https://doi.org/10.1111/hel.12386.

[7] G. Liechti, J.B. Goldberg, Helicobacter pylori relies primarily on the purine salvage pathway for purine nucleotide biosynthesis, J. Bacteriol. 194 (2012) 839–854, https://doi.org/10.1128/JB.05757-11.

[8] G.L. Mendz, A.J. Shepley, S.L. Hazell, M.A. Smith, Purine metabolism and the microaerophily of helicobacter pylori, Arch. Microbiol. 168 (1997) 448–456, https://doi.org/10.1007/s002030050521.

[9] M.I. Wojtyś, R. Jaźwiec, S. Kazazić, I. Leščić Ašler, P. Knežević, V. Aleksić Sabo, M. Luić, E.K. Jagusztyn-Krynicka, A. Bzowska, A comprehensive method for determining cellular uptake of purine nucleoside phosphorylase and adenylosuccinate synthetase inhibitors by H. Pylori, Appl. Microbiol. Biotechnol. 105 (2021) 7949–7967, https://doi.org/10.1007/s00253-021-11510-9.

[10] M. Bošnjaković, I. Leščić Ašler, Z. Štefanić, The role of phosphate binding in purine nucleoside phosphorylase of Helicobacter pylori, Croat. Chem. Acta 91 (2018) 171–175, https://doi.org/10.5562/cca3335.

[11] A. Bubić, N. Mrnjavac, I. Stuparević, M. Łyczek, B. Wielgus-Kutrowska, A. Bzowska, M. Luić, I. Leščić Ašler, In the quest for new targets for pathogen eradication: the adenylosuccinate synthetase from the bacterium helicobacter pylori, J. Enzyme Inhib. Med. Chem. 33 (2018) 1405–1414, https://doi.org/10.1080/14756366.2018.1506773.

[12] M. Narczyk, B. Bertoša, L. Papa, V. Vuković, I. Leščić Ašler, B. Wielgus-Kutrowska, A. Bzowska, M. Luić, Z. Štefanić, Helicobacter pylori purine nucleoside phosphorylase shows new distribution patterns of open and closed active site conformations and unusual biochemical features, FEBS J. 285 (2018) 1305–1325, https://doi.org/10.1111/febs.14403.

[13] Z. Štefanić, G. Mikleušević, M. Luić, A. Bzowska, I. Leščić Ašler, Structural characterization of purine nucleoside phosphorylase from human pathogen helicobacter pylori, Int. J. Biol. Macromol. 101 (2017) 518–526, https://doi.org/10.1016/j.ijbiomac.2017.03.101.

[14] A. Bzowska, E. Kulikowska, D. Shugar, Purine nucleoside phosphorylases: properties, functions, and clinical aspects, Pharmacol. Ther. 88 (2000) 349–425, https://doi.org/10.1016/S0163-7258(00)00097-8.

[15] M.M. Stayton, F.B. Rudolph, H.J. Fromm, Regulation, genetics, and properties of adenylosuccinate synthetase: a review, Curr. Top. Cell. Regul. 22 (1983) 103–141, https://doi.org/10.1016/B978-0-12-152822-5.50008-7.

[16] R.B. Honzatko, M.M. Stayton, H.J. Fromm, Adenylosuccinate synthetase: recent developments, Adv. Enzymol. Relat. Areas Mol. Biol. 73 (1999) 57–102.

[17] P. Krzyzek, E. Paluch, G. Gościniak, Synergistic therapies as a promising option for the treatment of antibiotic-resistant Helicobacter pylori, Antibiotics 9 (2020) 658–679, https://doi.org/10.3390/antibiotics9100658.

[18] S.D. Georgopoulos, V. Papastergiou, An update on current and advancing pharmacotherapy options for the treatment H. pylori infection, Expert. Opin. Pharmacother. 22 (2020) 729–741, https://doi.org/10.1080/14656566.2020.1845649.

[19] J.-Y. Choe, B.W. Poland, H.J. Fromm, R.B. Honzatko, Mechanistic implications from crystalline complexes of wild-type and mutant adenylosuccinate synthetases from Escherichia coli, Biochemistry 38 (1999) 6953–6961, https://doi.org/10.1021/bi990159s.

[20] K. Eaazhisai, R. Jayalakshmi, P. Gayathri, R.P. Anand, K. Sumathy, H. Balaram, M. R.N. Murthy, Crystal structure of fully ligated adenylosuccinate synthetase from plasmodium falciparum, J. Mol. Biol. 335 (2004) 1251–1264, https://doi.org/10.1016/j.jmb.2003.11.036.

[21] C.V. Iancu, T. Borza, H.J. Fromm, R.B. Honzatko, IMP, GTP, and 6-phosphoryl-IMP complexes of recombinant mouse muscle adenylosuccinate synthetase, J. Biol. Chem. 277 (2002) 26779–26787, https://doi.org/10.1074/jbc.M203730200.

[22] M.M. Bradford, A rapid and sensitive method for the quantitation of microgram quantities of protein utilizing the principle of protein-dye binding, Anal. Biochem. 72 (1976) 248–254, https://doi.org/10.1016/0003-2697(76)90527-3.

[23] D. Hayes, T. Laue, J. Philo, Program SEDNTERP: Sedimentation Interpretation Program, Alliance Protein Laboratories, Thousand Oaks (CA), 1995.

[24] P. Schuck, Size-distribution analysis of macromolecules by sedimentation velocity ultracentrifugation and lamm equation modelling, Biophys. J. 78 (2000) 1606–1619, https://doi.org/10.1016/S0006-3495(00)76713-0.

[25] F.B. Rudolph, H.J. Fromm, Initial rate studies of adenylosuccinate synthetase with product and competitive inhibitors, J. Biol. Chem. 244 (1969) 3832–3839, https://doi.org/10.1016/S0021-9258(17)36425-6.

[26] H.T.K. Britton, R.A. Robinson, Universal buffer solutions and the dissociation constant of veronal, J. Chem. Soc. (1931) 1456–1462, https://doi.org/10.1039/jr9310001456.

[27] W. Kabsch, XDS, Acta Crystallogr. D Biol. Crystallogr. 66 (Pt 2) (2010) 125–132, https://doi.org/10.1107/S0907444909047337.

[28] A. Vagin, A. Teplyakov, MOLREP: an automated program for molecular replacement, J. Appl. Crystallogr. 30 (1997) 1022–1025, https://doi.org/10.1107/S0021889897006766.

[29] D. Liebschner, P.V. Afonine, M.L. Baker, G. Bunkóczi, V.B. Chen, T.I. Croll, B. Hintze, L.W. Hung, S. Jain, A.J. McCoy, N.W. Moriarty, R.D. Oeffner, B.K. Poon, M.G. Prisant, R.J. Read, J.S. Richardson, D.C. Richardson, M.D. Sammito, O. V. Sobolev, D.H. Stockwell, T.C. Terwilliger, A.G. Urzhumtsev, L.L. Videau, C. J. Williams, P.D. Adams, Macromolecular structure determination using X-rays, neutrons and electrons: recent developments in phenix, Acta Crystallogr. D Struct. Biol. 75 (2019) 861–877, https://doi.org/10.1107/S2059798319011471.

[30] M.D. Winn, C.C. Ballard, K.D. Cowtan, E.J. Dodson, P. Emsley, P.R. Evans, R. M. Keegan, E.B. Krissinel, A.G.W. Leslie, A. McCoy, S.J. McNicholas, G. N. Murshudov, N.S. Pannu, E.A. Potterton, H.R. Powell, R.J. Read, A. Vagin, K. S. Wilson, Overview of the CCP4 suite and current developments, Acta Crystallogr. D Struct. Biol. 67 (2011) 235–242, https://doi.org/10.1107/S0907444910045749.

[31] A.J. McCoy, R.W. Grosse-Kunstleve, P.D. Adams, M.D. Winn, L.C. Storoni, R. J. Read, Phaser crystallographic software, J. Appl. Crystallogr. 40 (2007) 658–674, https://doi.org/10.1107/S0021889807021097.

[32] S. Bienert, A. Waterhouse, T.A.P. de Beer, G. Tauriello, G. Studer, L. Bordoli, T. Schwede, The SWISS-MODEL repository—new features and functionality, Nucl. Acids Res. 45 (2017) D313–D319, https://doi.org/10.1093/nar/gkw1132.

[33] R. Anandakrishnan, B. Aguilar, A.V. Onufriev, H++ 3.0: automating pK prediction and the preparation of biomolecular structures for atomistic molecular modeling and simulation, Nucl. Acids Res. 40 (W1) (2012) W537–W541, https://doi.org/10.1093/nar/gks375.

[34] J. Myers, G. Grothaus, S. Narayanan, A. Onufriev, A simple clustering algorithm can be accurate enough for use in calculations of pKs in macromolecules, Proteins 63 (2006) 928–938, https://doi.org/10.1002/prot.20922.
[35] J.C. Gordon, J.B. Myers, T. Folta, V. Shoja, L.S. Heath, A. Onufriev, H++: a server for estimating pKas and adding missing hydrogens to macromolecules, Nucl. Acids Res. 33 (2005) W368–W371, https://doi.org/10.1093/nar/gki464.
[36] J.A. Maier, C. Martinez, K. Kasavajhala, L. Wickstrom, K.E. Hauser, C. Simmerling, ff14SB: improving the accuracy of protein side chain and backbone parameters from ff99SB, J. Chem. Theory Comput. 11 (2015) 3696–3713, https://doi.org/10.1021/acs.jctc.5b00255.
[37] J. Wang, R.M. Wolf, J.W. Caldwell, P.A. Kollman, D.A. Case, Development and testing of a general amber force field, J. Comput. Chem. 56531 (2004) 1157–1174, https://doi.org/10.1002/jcc.20035.
[38] J. Wang, W. Wang, P.A. Kollman, D.A. Case, Automatic atom type and bond type perception in molecular mechanical calculations, J. Mol. Graph. Model. 25 (2006) 247–260, https://doi.org/10.1016/j.jmgm.2005.12.005.
[39] D.A. Case, T.A. Darden, T.E. Cheatham III, C.L. Simmerling, J. Wang, R.E. Duke, R. Luo, M. Crowley, R.C. Walker, W. Zhang, K.M. Merz, B. Wang, S. Hayik, A. Roitberg, G. Seabra, I. Kolossváry, K.F. Wong, F. Paesani, J. Vanicek, X. Wu, S. R. Brozell, T. Steinbrecher, H. Gohlke, L. Yang, C. Tan, J. Mongan, V. Hornak, G. Cui, D.H. Mathews, M.G. Seetin, C. Sagui, V. Babin, P.A. Kollman, Amber 10, University of California, San Francisco, 2008.
[40] R.L. Davidchack, R. Handel, M.V. Tretyakov, Langevin thermostat for rigid body dynamics, J. Chem. Phys. 130 (2009), 234101, https://doi.org/10.1063/1.3149788.
[41] R.L. Davidchack, T.E. Ouldridge, M.V. Tretyakov, New langevin and gradient thermostats for rigid body dynamics, J. Chem. Phys. 142 (2015), 144114, https://doi.org/10.1063/1.4916312.
[42] H.J.C. Berendsen, J.P.M. Postma, W.F. Van Gunsteren, A. Dinola, J.R. Haak, Molecular dynamics with coupling to an external bath, J. Chem. Phys. 81 (1984) 3684, https://doi.org/10.1063/1.448118.
[43] W. Humphrey, A. Dalke, K. Schulten, VMD: visual molecular dynamics, J. Mol. Graph. 14 (1996) 33–38, https://doi.org/10.1016/0263-7855(96)00018-5.
[44] J. Eargle, D. Wright, Z. Luthey-Schulten, Multiple alignment of protein structures and sequences for VMD, Bioinformatics 22 (2006) 504–506, https://doi.org/10.1093/bioinformatics/bti825.
[45] D. Frishman, P. Argos, Knowledge-based protein secondary structure assignment, Proteins Struct. Funct. Genet. 23 (1995) 566–579.
[46] A. Varshney, F.P. Brooks, W.V. Wright, Computing smooth molecular surfaces, IEEE Comput. Graph. Appl. 14 (1994) 19–25, https://doi.org/10.1109/38.310720.
[47] R. Sharma, M. Zeller, V.I. Pavlovic, T.S. Huang, Z. Lo, S. Chu, Y. Zhao, J.C. Phillips, K. Schulten, Speech/gesture interface to a visual-computing environment, IEEE Comput. Graph. Appl. 20 (2000) 29–37, https://doi.org/10.1109/38.824531.
[48] W.T. Booth, C.R. Schlachter, S. Pote, N. Ussin, N.J. Mank, V. Klapper, L. R. Offermann, C. Tang, B.K. Hurlburt, M. Chruszcz, Impact of an N-terminal polyhistidine tag on protein thermal stability, ACS Omega 3 (2018) 760–768, https://doi.org/10.1021/acsomega.7b01598.
[49] K.A. Majorek, M.L. Kuhn, M. Chruszcz, W.F. Anderson, W. Minor, Double trouble – buffer selection and his-tag presence may be responsible for nonreproducibility of biomedical experiments, Protein Sci. 23 (2014) 1359–1368, https://doi.org/10.1002/pro.2520.
[50] M. Carson, D.H. Johnson, H. McDonald, C. Brouillette, L.J. DeLucas, His-tag impact on structure, Acta Crystallogr. D Struct. Biol. 63 (2007) 295–301, https://doi.org/10.1107/S0907444906052024.
[51] E.A. Kaczka, C.O. Gitterman, E.L. Dulaney, K. Folkers, Hadacidin, a new growth-inhibitory substance in human tumor systems, Biochemistry 1 (1962) 340–343, https://doi.org/10.1021/bi00908a022.
[52] C. Soans, H.J. Fromm, Studies of ligand binding to Escherichia coli adenylosuccinate synthetase, Arch. Biochem. Biophys. 291 (1991) 107–112, https://doi.org/10.1016/0003-9861(91)90111-U.
[53] K. Dalziel, Physical significance of michaelis constants, Nature 196 (1962) 1203–1205, https://doi.org/10.1038/1961203b0.
[54] R.B. Honzatko, H.J. Fromm, Structure-function studies of adenylosuccinate synthetase from Escherichia coli, Arch. Biochem. Biophys. 370 (1999) 1–8, https://doi.org/10.1006/abbi.1999.1383.
[55] P.T. Wingfield, N-terminal methionine processing, Curr. Protoc. Protein Sci. 88 (2017) 6.14.1-3, https://doi.org/10.1002/cpps.29.
[56] E. Krissinel, K. Henrick, Secondary-structure matching (SSM), a new tool for fast protein structure alignment in three dimensions, Acta Crysttallogr. D Biol. Crystallogr. 60 (2004) 2256–2268, https://doi.org/10.1107/S0907444904026460.
[57] E. Krissinel, K. Henrick, Inference of macromolecular assemblies from crystalline state, J. Mol. Biol. 372 (2007) 774–777, https://doi.org/10.1016/j.jmb.2007.05.022.
[58] O.A. Moe, J.F. Baker-Malcolm, W. Wang, C. Kang, H.J. Fromm, R.F. Colman, Involvement of arginine 143 in nucleotide substrate binding at the active site of adenylosuccinate synthetase from Escherichia coli, Biochemistry 35 (1996) 9024–9033, https://doi.org/10.1021/bi960426j.
[59] Z. Hou, W. Wang, H.J. Fromm, R.B. Honzatko, IMP alone organizes the active site of adenylosuccinate synthetase from Escherichia coli, J. Biol. Chem. 277 (2002) 5970–5976, https://doi.org/10.1074/jbc.M109561200.
[60] M.M. Silva, B.W. Poland, C.R. Hoffman, H.J. Fromm, R.B. Honzatko, Refined crystal structures of unligated adenylosuccinate synthetase from Escherichia coli, J. Mol. Biol. 254 (1995) 431–446, https://doi.org/10.1006/jmbi.1995.0629.
[61] W. Wang, A. Gorrell, Z. Hou, R.B. Honzatko, H.J. Fromm, Ambiguities in mapping the active site of a conformationally dynamic enzyme by directed mutation, J. Biol. Chem. 273 (1998) 16000–16004, https://doi.org/10.1074/jbc.273.26.16000.
[62] N. Tibrewal, G.I. Elliott, Design, synthesis and evaluation of AdSS bisubstrate inhibitors, ChemMedChem 15 (2020) 2269–2272, https://doi.org/10.1002/cmdc.202000498.
[63] J.T. Han, H.B. Dong, Z.H. Xu, J.M. Wang, M.A. Wang, Synthesis and activity of novel acylthiourea with hydantoin, Int. J. Mol. Sci. 14 (2013) 19526–19539, https://doi.org/10.3390/ijms141019526.
[64] F.D.S. Ribeiro, G.S. de Araujo, M.G.A. Mendes, T.C. Daboit, L.M. Brito, C. Pessoa, L. R.M. de Lima, R.C.M. de Paula, R.S. Bastos, J.A. Rocha, E.D. Sa, T.C. de Oliveira, A. C.D. Oliveira, J.L.S. Sobrinho, J.R.D.D. Leite, A.R. de Araujo, D.A. da Silva, Structural characterization, antifungal and cytotoxic profiles of quaternized heteropolysaccharide from anadenanthera colubrine, Int. J. Biol. Macromol. 165 (2020) 279–290, https://doi.org/10.1016/j.ijbiomac.2020.09.087.
[65] R.Y.B. Nugraha, I.F.D. Faratisha, K. Mardhiyyah, D.G. Ariel, F.F. Putri, S. Nafisatuzzamrudah, T.W. Winarsih, L.E.Fitri Sardjono, Antimalarial properties of isoquinoline derivative from streptomyces hygroscopicus subsp. Hygroscopicus: an in silico approach, Biomed. Res. Int. (2020), https://doi.org/10.1155/2020/6135696.